# Formation of CdS Nanoparticles within Modified MCM-41 and SBA-15

**Wei Xu, Yanting Liao, and Daniel L. Akins***

*Center for Analysis of Structures and Interfaces (CASI), Department of Chemistry, The City College of The City University of New York, New York, New York 10031*

*Received: February 16, 2002; In Final Form: July 10, 2002*

Cadmium sulfide nanoparticles were formed within both modified mesoporous aluminosilicate MCM-41 and siliceous SBA-15. Syntheses involved the formation of a monolayer of silylation reagent, (3-mercaptopropyl)-trimethoxysilane, on the surfaces of both MCM-41 and SBA-15, which served to preposition the sulfide source within the mesoporous channels. A source of Cd ions was then added, leading to reaction with the prepositioned sulfide and with added $H_2S$ to result in occluded CdS nanoparticles. The average diameters of nanoparticles of CdS formed within the mesochannels of MCM-41 and SBA-15, as characterized by XRD and UV−vis diffuse reflectance, were ca. 2.1 and 3.4 nm, respectively. The thicker wall and larger pore size of SBA-15 compared to MCM-41, represents a more stable matrix for forming the occluded nanoparticle, as indicated by the stability of the XRD patterns for the nanocomposite utilizing SBA-15 versus that when MCM-41 was used. Also, from Raman spectra for the CdS/MCM-41 system, the relative intensities of the fundamental band and the overtone band were found to differ for the bulk and nanoparticle samples. We discussed this observation in terms of electronic anharmonicity. Furthermore, blue shifts for both fundamental and overtone Raman bands were observed when compared to bulk CdS: 303 vs 299 $cm^{-1}$ and 605 vs 599 $cm^{-1}$, respectively. We rationalized this observation in terms of CdS lattice compression and/or sulfide vacancies, particularly at the interface between the nanoparticle and the mesoporous cage matrix. We further suggest that the stoichiometry for the nanoparticle is more appropriately $CdS_{1-x}$. Lastly, photoluminescence shifts were rationalized on the basis of nanoparticle size, incident excitation intensity, as well as temperature.

## I. Introduction

Semiconductor nanoparticles, also referred to as quantum dots, have garnered enormous attention in recent years. And, in particular, compound II−VI semiconductor nanoparticles have been a focus because they are optoelectronic materials with functionalities in flat-panel displays, field-effect thin-film transistors, light-emitting diodes, and single-electron transistors.[1−5] Since the properties of semiconductor nanocrystals depend both on dimension and superlattice structure, it is important to control size and shape in their syntheses and to arrange them over useful dimensions.

Syntheses of nanoparticles within mesoporous silica, such as MCM-41 and SBA-15, which are one-dimensional, hexagonally arranged porous materials of highly uniform dimensions, represent a constricted growth process that provides control of nanoparticle dimensions. Three methodologies have been developed to transport precursor molecules or ions for assembly of nanoparticles inside the channels of such materials: (a) direct impregnation,[6,7] (b) modification of the surface walls followed by loading of precursors through affinity interaction,[8,9] and (c) ion-exchange reaction.[10] Without doubt, the direct impregnation method alone, without the functionalizing of the surface walls, has generally proven unsuccessful in obtaining meaningful amounts of nanocrystals within the channels of silicates;[6,7] in particular, in the case of synthesis of CdS within the channels, it has been found that under high loading and evaporation to remove solvent, although some of CdS nanoparticles are formed within the channels of MCM-41, the majority of CdS particles are located outside of the porous structure.[8,9] However, the ion-exchange reaction approach, as modified by passivating the external surface to facilitate ion-exchange incorporation of a reagent ion, shows promise, but the effectiveness of affinity loading the channels of the silicates is uncertain.[10] We have deduced that the most promising approach is built around (b) above, and, in this paper, apply the concept of functionalizing the interior wall of mesoporous MCM-41 and SBA-15 for the synthesis of encapsulated CdS by choosing a silylation reagent that incorporates one of the reactant ions.

Examination of the literature indicates that interest has been shown in the preparation of CdS nanoparticles within MCM-41. However, little in the way of spectroscopic analyses has been applied to the characterization of the nanocomposite system. In this paper, we acquire UV−vis absorption, photoluminescence, and Raman spectra of nanocomposites consisting of CdS within both MCM-41 and SBA-15. We also study the effects of temperature, incident intensity, and particle size on the measured spectra, and deduce that sulfur vacancies are present within the mesoporous channel, which result in the stoichiometry of the occluded nanoparticles as being $CdS_{1-x}$, instead of the 1:1 stoichiometry (as occurs for bulk CdS) that has been reported in the literature.

## II. Experimental Section

**Synthesis of Functionalized MCM-41 and SBA-15.** Polycrystalline powders of the mesostructural aluminosilicate MCM-41 were prepared by using cetyltrimethylammonium bromide (CTAB) as the template.[11,12] Briefly, $Na_2SiO_3$ solution (Aldrich, ∼27% $SiO_2$) and a calculated amount of $NaAlO_2$ (Alfa) solution (Si/Al = 10) were added to CTAB (Aldrich) solution according to the molar composition ratio $5SiO_2$:$0.25Al_2O_3$:CTAB:$610H_2O$. The pH was lowered to 11 with 2 M $H_2SO_4$, and the mixture was stirred for more than 3 h at about 318 K. The temperature

10.1021/jp025651r CCC: $22.00 
Published on Web 10/08/2002

was then raised to 373 K, and the reaction allowed for 72 h in a Teflon-lined autoclave. The resulting precipitate was filtered, washed thoroughly with distilled water, and calcined in air at 773 K to obtain the final product, MCM-41 (see discussions below of XRD patterns).

Polycrystalline powders of the mesostructural siliceous SBA-15 were synthesized by using a triblock copolymer as the template.[13−15] Specifically, in our case, 6.0 g of triblock poly(ethylene oxide)−poly(propylene oxide)−poly(ethylene oxide) ($EO_{20}PO_{70}EO_{20}$, also referred to as Pluronic 123, Aldrich) was dissolved in 170 mL of 2 M aqueous HCl with stirring. Next, at room temperature, 13.5 mL of tetraethyl orthosilicate (TEOS, Aldrich) was added dropwise to the resultant solution. The mixture was stirred for 24 h at ca. 313 K, then the temperature was raised to ca. 373 K, and the reaction allowed to stand for 48 h in a Teflon-lined autoclave. The resulting precipitate, as in the case of the MCM-41 synthesis, was filtered, dried, and calcined in air at ca. 773 K to obtain the final product, SBA-15.

Both MCM-41 and SBA-15 were modified by subsequent treatment that involved the functionalizing and rigidizing of the inner surface walls of the silicates through reaction with the silylation reagent (3-mercaptopropyl)trimethoxysilane (MPTMS; $HS-(CH_2)_3-Si-(CH_3O)_3$). The method used is similar to that in our prior studies,[16,17] in which (aminopropyl)-triethoxysilane (APTES; $NH_2-(CH_2)_3-Si-(C_2H_5O)_3$) was used as silylation reagent. The method involved, briefly, taking about 1.5 g of either calcined MCM-41 or SBA-15 and mixing it with a chloroform solution of MPTMS (100 mL, 0.4 M), which was stirred overnight at room temperature. The precipitate was filtered and washed with chloroform and dichloromethane.

**Formation of CdS Nanoparticles.** A typical preparation of occluded cadmium sulfide nanoparticles within modified silicate involved stirring and refluxing a mixture of 600 mg of modified MCM-41 or SBA-15 with 100 mL of cadmium(II) methanol solution (60 mg of $Cd(OAc)_2{\bullet}2H_2O$ dissolved in 100 mL of HPLC grade methanol) for 24 h. The solution was then centrifuged and the transparent aqueous solution decanted. The residue was washed with methanol to remove $Cd^{2+}$ from the external surface and then dried at 333 K in a vacuum. The final step involved the treatment with a flow of 5 vol % $H_2S$ in $N_2$ for 6 h at room temperature. The composites involving MCM-41 and SBA-15 are hereinafter also referred to as CdS/MCM-41 and CdS/SBA-15, respectively.

**Instrumentation.** Absorption spectra were recorded using a Perkin-Elmer Lambda 18, UV−vis−NIR spectrometer. The X-ray diffraction (XRD) instrument used was a Rigaku diffractometer using Cu $K_{\alpha 1}$ (0.154 nm) X-rays; typically run at a voltage of 40 kV and current of 30 mA. Photoluminescence was taken using a He−Cd laser, with the emission at 325 nm as the excitation wavelength. For temperature studies, the samples were mounted on the coldfinger of a Janis cryogenic system (Model ST-300; which allowed cooling to 78 K using liquid nitrogen); prior to cooling, the system was pumped to $\sim 10^{-4}$ Torr. For incident intensity studies, the excitation laser intensity was varied by using a set of neutral density filters whose transmissions ranged from 50% to 3%. Luminescence was collected by optical lenses, focused on the slit of a Spex 1680-B spectrometer, and detected with a photomultiplier tube.

Raman spectra of bulk CdS (Aldrich, $< 5\ \mu$m grains) and nanocomposite grains were excited with laser radiation of wavelengths 457.9, 488.0, and 514.5 nm, from a Coherent Innova 200 argon-ion laser. The excitation power was maintained at 120 mW, and the Raman scattering was collected and dispersed by a Spex 1877, 0.6-meter spectrometer. A cooled (140 K) Spex Spectrum-1 CCD camera was coupled to the spectrometer and used as the detector.

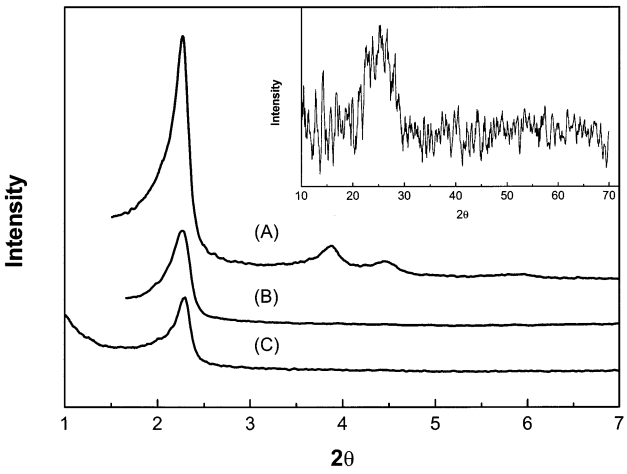


**Figure 1.** XRD patterns of (A) calcined MCM-41, (B) modified MCM-41, and (C) CdS/MCM-41. Inset shows diffraction in region corresponding to CdS.

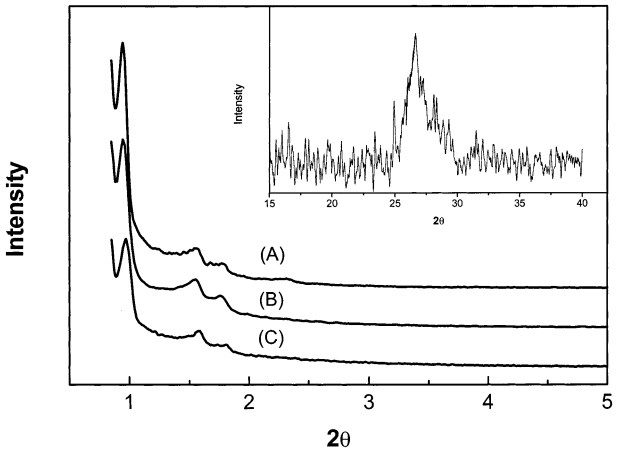


**Figure 2.** XRD patterns of (A) calcined SBA-15, (B) modified SBA-15, and (C) CdS/SBA-15. Inset shows diffraction in region corresponding to CdS.

## III. Results and Discussion

A series of XRD patterns for pristine calcined MCM-41, modified MCM-41, and cadmium sulfide nanoparticles within MCM-41 are shown in Figure 1. Similar measurements for the series involving SBA-15 are shown in Figure 2.

The XRD patterns of the composites containing CdS (i.e., CdS/MCM-41 and CdS/SBA-15) show strong (100) peaks, suggesting that framework stability is exhibited when CdS is encapsulated within modified MCM-41 and SBA-15. Moreover, one can deduce that formation of CdS nanoparticles within the channels of modified MCM-41 and SBA-15 does not decrease the framework integrity of the two hosts (see parts B and C of Figure 1 and Figure 2). Furthermore, for the SBA-15 system (as shown in Figure 2) one observes that all XRD patterns for the series also show strong (110) and (200) peaks, and that the relative intensities of these peaks are essentially constant, indicating a more integrated structure than that involving MCM-41. We attribute the more integrated character of the SBA-15 system to the thicker intercore spacing that it possesses ($\sim$40 Å) when compared to that of MCM-41 ($\sim$10 Å).[15]

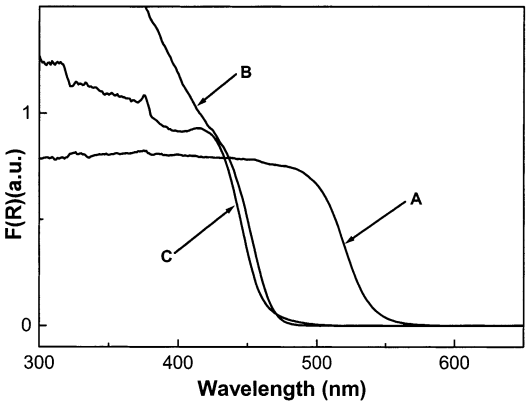


**Figure 3.** Diffuse reflectance UV−vis spectra of CdS in various environments: (A) bulk CdS, (B) CdS/SBA-15, and (C) CdS/MCM-41.

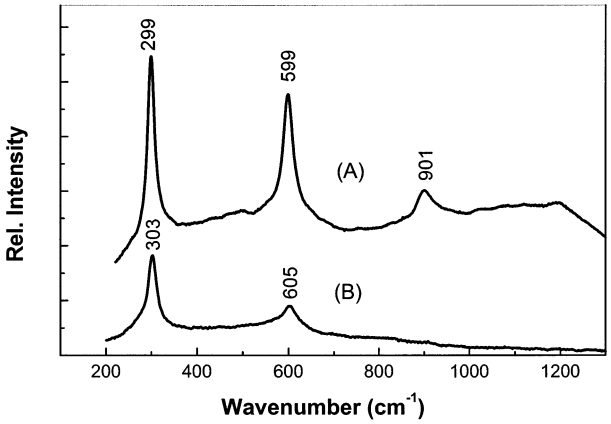


**Figure 4.** Room-temperature resonant Raman spectra of (A) bulk CdS, excitation wavelength = 514.5 nm; (B) nanocomposite CdS/MCM-41, excitation wavelength = 457.9 nm.

Returning to Figure 1, we note the inset that shows the wide-angle XRD pattern for CdS/MCM-41 that contains cadmium sulfide nanoparticles. The mean particle size can be determined from the X-ray diffraction position and the peak width using the Scherrer formula, $d = 0.941\lambda/B\cos\theta_B$, where $d$ is the mean diameter of the particle, $\lambda$ is the wavelength of the Cu $K_{\alpha 1}$ line (0.154 nm), $\theta_B$ is the angle between the incident beam and the reflection lattice planes, and $B$ is the width (in radians) of the diffraction peak. From the width and position of the diffraction peak, the average size of nanoparticles is found to be ca. 21 Å, which is concordant with the pore size of modified MCM-41, which was determined in a prior study[16] in which (aminopropyl)-triethoxysilane (APTES) was the silylation reagent. Similarly, from the inset in Figure 2, the average size of CdS nanoparticles within SBA-15 is calculated to be ca. 34 Å.

Diffuse reflectance (DR) UV−vis spectra of the series bulk-CdS, CdS/SBA-15, CdS/MCM-41 have been acquired (see Figure 3, parts A, B, and C, respectively). An obvious blue shift in the absorption band-edge (close to 550 nm) occurs as the CdS particle's size decreases. The direction of the blue shift is in agreement with quantum confinement effects due to decreasing particle size.

Representative resonance Raman spectra for bulk CdS, excited with 514 nm radiation, and CdS nanoparticles occluded within MCM-41 (i.e., CdS/MCM-41), excited with 457.9 nm radiation, are shown in Figure 4, parts A and B, respectively. Both spectra contain a longitudinal optical (LO) phonon mode at ca. 300 $cm^{-1}$ as well as the first overtone band at ca. 600 $cm^{-1}$. The bulk sample, however, exhibits higher overtones,

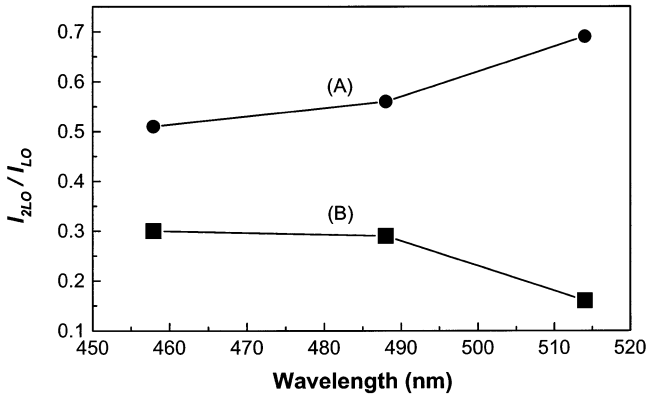


**Figure 5.** Dependence of relative intensities ($I_{2LO}/I_{LO}$) on excitation wavelength: (A) bulk CdS, (B) CdS/MCM-41.

**TABLE 1: Fundamental and Overtone Raman Bands Positions as a Function of Excitation Frequency for Bulk CdS and CdS Occluded in MCM-41**

| | $\lambda_{ex}$ = 457.9 nm | | | $\lambda_{ex}$ = 488.0 nm | | | $\lambda_{ex}$ = 514.5 nm | | |
|---|---|---|---|---|---|---|---|---|---|
| samples | LO | 2LO | $I_{2LO}/I_{LO}$ | LO | 2LO | $I_{2LO}/I_{LO}$ | LO | 2LO | $I_{2LO}/I_{LO}$ |
| bulk CdS | 300 | 601 | 0.51 | 299 | 604 | 0.56 | 299 | 599 | 0.69 |
| CdS/MCM-41 | 302 | 605 | 0.30 | 302 | 607 | 0.29 | 303 | 605 | 0.16 |

likely indicating strong electronic anharmonicity. The relative intensities of the first overtone band and the fundamental band (e.g., $I_{2LO}/I_{LO}$, where $I_{2LO}$ is the peak intensity of the first overtone and $I_{LO}$ that of the fundamental) might be expected to provide insight on the structure of the CdS nanoparticle. Table 1 provides the Raman numerical results pertaining to a comparison of overtone- and fundamental-band measurements for bulk CdS and nanocomposite CdS/MCM-41, while Figure 5 provides a plot of the relative intensities ($I_{2LO}/I_{LO}$) versus excitation wavelength. As shown in Figure 5 and Table 1, for bulk CdS, $I_{2LO}/I_{LO}$ is always greater than the same ratio for the composite for all excitation wavelengths. Moreover, the ratio is found to increase as the exciting frequency approaches the absorption band-edge, which is shown in Figure 3, for both bulk and composite samples. We note, however, that the ratio of Raman intensities for the composite, when resonantly excited, giving $I_{2LO}/I_{LO} = 0.30$, is less than the ratio for the bulk ($I_{2LO}/I_{LO} = 0.51$), despite the fact that the exciting frequency is off-resonance for the latter. Hence, it appears, for the bulk sample, that the electronic anharmonicity plays a greater role in determining overtone intensity than does the Franck−Condon resonance contribution to the overtone intensity for the composite. Of course, $I_{2LO}/I_{LO}$ is enhanced for both the bulk and composite samples as resonance is approached, as shown in Figure 5. We will discuss the implications of this finding in a later publication.

Another aspect of the Raman measurements are blue shifts of both the fundamental and overtone bands for the nanoparticle-composite vis-à-vis the respective bands for bulk CdS (see Table 1). An obvious explanation for the blue shifts is lattice compression resulting from the constricted dimension of the pore in which the nanoparticle is formed. A second explanation might be associated with site vacancies such as discussed by Spanier et al.[18] in their study involving $CeO_2$ nanoparticles. Spanier et al.,[18] in which an approach developed by McBride et al.[19] was applied, suggested that the existence of an oxygen vacancy site for $CeO_2$ can lead to a blue shift of Raman bands, and that the stoichiometric product is more appropriately represented by the formula $CeO_{2-y}$, where $y$ corresponds to an "impurity" concentration. In our case, during the formation process of CdS

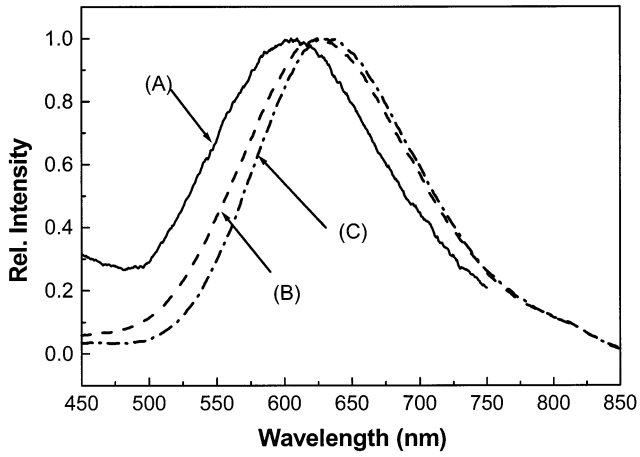


**Figure 6.** Low-temperature (77 K) photoluminescence spectra of (A) bulk CdS, (B) CdS/SBA-15, and (C) CdS/MCM-41. Excitation wavelength and radiation power of 325 nm and 36 mW, respectively.

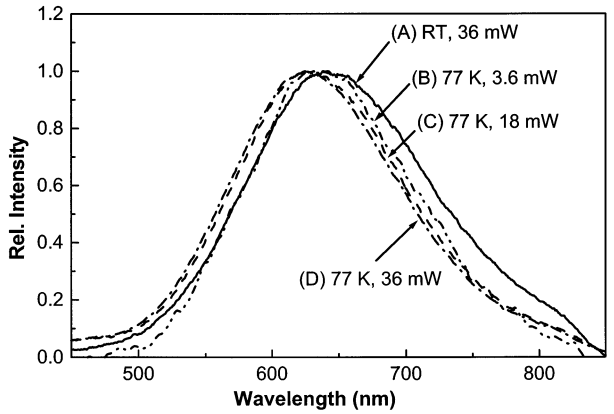


**Figure 7.** Temperature and excitation power dependence of photoluminescence for nanocomposite CdS/SBA-15. (A) Room temperature with excitation power of 36 mW; (B) 77 K with excitation power of 3.6 mW; (C) 77 K with excitation power of 18 mW; and (D) 77 K with excitation power of 36 mW.

nanoparticles with $H_2S$, some Cd(II) cations might be expected to incorporate and become stabilized within the nanocrystals by affinitive interaction with sulfur on the surface walls of the functionalized MCM-41. As a result, interfacial sulfur vacancies are to be expected for the CdS nanoparticles and the stoichiometric description of the nanoparticle would be $CdS_{1-x}$, where $x$ is related to the vacancy concentration.

Both explanations for the blue shifts of the Raman bands suggest the existence of possible surface trap sites, which would likely evidence themselves in photoluminescence spectra—since electron−hole pair recombination from trap states results in Stokes shifted luminescence.[20,21] To examine this point, we acquired low-temperature photoluminescence spectra of bulk CdS and nanocomposite systems. As indicated in Figure 6, the photoluminescences from the composites exhibit substantial Stokes shifts when compared to their respective absorption band edges; moreover, the shift increases with a decrease in the nanoparticle's diameter. Hence, the observed photoluminescence likely derives from recombination of holes and electrons at surface traps whose concentrations increase with decreasing particle size. Our plan for a future study is to measure lifetimes of the excitons and the effect of added $S^{2-}$ on photoluminescence, in our composite systems, to verify the role of surface traps.

To complete our experimental measurements in the present study, we also examined temperature and excitation-intensity dependences of photoluminescence from the CdS/SBA-15 composite (see Figure 7), to gauge whether our nanoparticles behave in a way similar to that of others reported in the literature. In this regard we observed that at a fixed excitation power of 36 mW, but with temperature of either RT or 77 K, a difference in peak position occurs, 638 nm vs 624 nm, respectively (compare parts A and D of Figure 7). This finding is consistent with expectations since an increase in temperature is anticipated to cause thermal expansion of the lattice and a concomitant diminution of electron−phonon interactions, resulting in lowered band gap energy.[22] Also, we note from Figure 7 that with increasing incident excitation intensity, at the temperature of 77 K, the photoluminescence peak shifts to higher energy, i.e., blue shift (see parts B, C, and D of Figure 7). This finding is also consonant with expectations, since, based on exciton recombination lifetime measurements,[23] increasing excitation intensity leads to the filling of lower energy exciton states, and the populating of higher exciton states, which, in turn, is reflected in a blue shift of the photoluminescence.

## IV. Conclusion

The combination of XRD, Raman scattering, UV−vis absorption, and photoluminescence measurements indicates that we have formed cadmium sulfide nanoparticles within the channels of modified MCM-41 and SBA-15, and that the nanoparticle formed within MCM-41 is smaller than that formed in SBA-15 (which have cage diameters of ca. 2.1 and 3.4 nm, respectively). The functionalization of the interior wall of the mesostructure utilizing a sulfide containing alkoxysilane reagent facilitates incorporation of Cd(II) cations and the formation of cadmium sulfide. Comparison of fundamental and overtone band positions relative to those of bulk CdS for encapsulated CdS, suggests that both constricted vibrations of the CdS nanoparticles within the mesoporous materials as well as interfacial sulfur vacancies, leading to a stoichiometry for the nanoparticles as indicated in the chemical formula $CdS_{1-x}$, play roles in the direction of the shifts. Moreover, we deduce that electronic anharmonicity plays a large role in determining the relative intensity of the fundamental and overtone bands. We have also observed the effect of nanoparticle size on photoluminescence peak wavelength, deducing that the smaller nanoparticle has more surface trap states, resulting in a greater red shift in its exciton peak emission wavelength. Also, in our study of the effects of excitation power and temperature on photoluminescence of CdS encapsulated within SBA-15, we have deduced that the expected lattice expansion effect with increased temperature and the population of higher exciton states with increased intensity explain our observations for CdS nanoparticles prepared by the unique procedure described herein.

**Acknowledgment.** The NSF supported this work, in part, through the following awards: (1) IGERT program under Grant No. DGE-9972892; (2) CIRE program under Grant No. CHE-9872777; and (3) MRSEC program under Grant No. DRM-9809687. One of us (D.L.A.) also thanks a colleague (Dr. Maria C. Tamargo) for use of her XRD and photoluminescence instruments.

## References and Notes

(1) Brus, L. E., Efros, Al., Itoh, T., Eds. Spectroscopy of Isolated and Assembled Semiconductor Nanocrystals. *J. Lumin.* **1996**, *76*, 1 (special issue).

(2) Alivisatos, A. P. *Science* **1996**, *271*, 933.

(3) Colvin, V. L.; Schlamp, M. C.; Alivisatos, A. P. *Nature* **1994**, *370*, 354.

(4) Klein, D. L.; Roth, R.; Lim, A. K. L.; Alivisatos, A. P.; McEuen, P. L. *Nature* **1997**, *389*, 699.
(5) Ridley, B. A.; Nivi, B.; Jacobson, J. M. *Science* **1999**, *286*, 746.
(6) Chen, L.; Klar, P.; Heimbrodt, W.; Brieler, F.; Fröba, M. *Appl. Phys. Lett.* **2000**, *76*, 3531.
(7) Chen, L.; Klar, P.; Heimbrodt, W.; Brieler, F.; Fröba, M.; Nidda, H.; Loidl, A. *Physica E* **2001**, *10*, 368.
(8) Wellmann, H.; Rathoussky, J.; Wark, M.; Zukal, A.; Schulz-Ekloff, G. *Microporous Mesoporous Mater.* **2001**, *44*−*45*, 419.
(9) Hirai, T.; Okubo, H.; Komasawa, I. *J Phys. Chem. B* **1999**, *103*, 4228.
(10) Zhang, Z.; Dai, S.; Fan, X.; Blom, D.; Pennycook, S. J.; Wei, Y. *J Phys. Chem. B* **2001**, *105*, 6755.
(11) Kresge, C. T.; Leonowicz, M. E.; Roth, W. J.; Vartuli, J. C.; Beck, J. S. *Nature* **1992**, *359*, 710.
(12) Beck, J. S.; Vartuli, J. C.; Roth, W. J.; Leonowicz, M. E.; Kresge, C. T.; Schmitt, K. D.; Chu, C. T.-W.; Olsen, D. H.; Sheppard, E. W.; McCullen, B.; Higgins, J. B.; Schlenker, J. L. *J. Am. Chem. Soc.* **1992**, *114*, 10834.
(13) Zhao, D.; Feng, J.; Huo, Q.; Melosh, N.; Fredrickson, G. H.; Chmelka, B. F.; Stucky, G. D. *Science* **1998**, *279*, 548.
(14) Zhao, D.; Huo, Q.; Feng, J.; Chmelka, B. F.; Stucky, G. D. *J. Am. Chem. Soc.* **1998**, *120*, 6024.
(15) Xu, W.; Akins, D. L. *J. Phys. Chem. B* **2002**, *106*, 1943.
(16) Xu, W.; Guo, H.; Akins, D. L. *J. Phys. Chem. B* **2001,** *105*, 1543.
(17) Xu, W.; Guo, H.; Akins, D. L. *J. Phys. Chem. B* **2001**, *105*, 7686.
(18) Spanier, J. E.; Robinson, R. D.; Zhang, F.; Chan, S.-W.; Herman, I. P. *Phys. Rev. B* **2001**, *64*, 245407.
(19) McBride, I. R.; Hass, K. C.; Poindexter, B. D.; Weber, W. H. *J. Appl. Phys.* **1994**, *76*, 2435.
(20) Murphy, C. J.; Coffer, J. L. *Appl. Spectrosc.* **2002**, *56* (1), 21A.
(21) Kamalov, V. F.; Little, R.; Logunov, S. L.; M. A. El-Sayed. *J. Phys. Chem.* **1996**, *100*, 6381.
(22) Perna, G.; Capozzi, V.; Pagliara, S.; Ambrico, M. *Appl. Surf. Sci.* **2000**, *154*, 238.
(23) Matsuura, D.; Kanemitsu, Y.; Kushida, T.; White, C. W.; Budai, J. D.; Meldrum, A. *Jpn. J. Appl. Phys.* **2000**, *40*, 2092.